

An equivalent circuit approach to organic solar cell modelling

Ali Cheknane^{a,*}, Hikmat S. Hilal^b, Fayçal Djeflal^c,
Boumediène Benyoucef^d, Jean-Pierre Charles^e

^aLaboratoire d'Etude et Développement des Matériaux Semiconducteurs et Diélectriques, Université Amar Telidji de Laghouat,
BP 37G, route de Ghardaïa, Laghouat (03000), Algérie

^bAn-Najah N. University, P.O. Box 7, Nablus, West Bank, Palestine

^cLEA, Department of Electronics, University of Batna, Algeria

^dUnité de Recherche Matériaux et Energies Renouvelables, Université Abou Bakar Belkaid de Tlemcen, Algérie

^eLMOPS-CNRS UMR 7132, SUPELEC, 2 rue Edouard Belin, 57070 Metz, France

Received 25 December 2007; accepted 25 January 2008

Available online 14 March 2008

Abstract

In this paper, we present a simulation study for a newly prepared organic solar cell, based on a composite of poly (2-methoxy-5-(2'-ethylhexyloxy)-1, 4-phenylenevinylene (MEH-PPV) with [6, 6]-phenyl C₆₀ butyric acid methyl ester (PCBM). Photo-current density vs. voltage ($J-V$) characteristics, for the cell, which were experimentally studied earlier, have been revisited here. The results indicated that the conduction mechanism in the organic solar cell is strongly influenced by the excitonic diffusion. Sound correlation, between theoretical and experimental photo-current density vs. voltage ($J-V$) plots, has been achieved. Moreover, the simulation clearly demonstrates that the performance of the tested device can be described, with sound accuracy, by a two-diode-equivalent model.

© 2008 Elsevier Ltd. All rights reserved.

Keywords: MEH-PPV/PCBM; Organic solar cell; Exciton; Photo-current density vs. voltage plots; Modeling; Two-diode model

1. Introduction

Organic polymer photovoltaics (PV), are showing early promise as an alternative option in the solar PV technology. Although it is only early days yet for the technology, the vision is for the mass production of these materials by simple roll-to-roll or printing processes with lower thermal price and less stringent requirements than traditional inorganic semiconductor technology. The production potential, for a single process line based on printing, may possibly exceed 1000 m² per hour [1].

The most promising designs are based on a combination of electron-donating and electron-accepting molecular materials, so as to emulate p–n heterojunctions. One class of particular interest is the donor–acceptor heterojunction formed from a blend of a conjugated polymer with a fullerene derivative [2–13].

An example of promising organic solar cells, is that based on poly (2-methoxy-5-(2'-ethylhexyloxy)-1,4-phenylenevinylene and [6,6]-phenyl C₆₀ butyric acid methyl ester heterojunction (MEH-PPV/PCBM), which has been prepared and experimentally studied earlier. The cell showed 2.9% power conversion efficiency under 100 mW/cm² illumination intensity as reported by Nunzia et al. [12] and by others [13]. Li et al. reported lower conversion efficiency for similar cells based on MEH-PPV and polymers with substituents containing C₆₀ moieties [14]. Due to its special features and applicability in photovoltaic devices, the MEH-PPV has been heavily studied from different points of view, namely: carrier mobility [15], ability to sensitize titania [16], LED devices [17], luminescence [18–23] and other characteristics. This interest reflects the future expectations from the MEH-PPV/PCBM organic solar cell.

The future of the MEH-PPV/PCBM organic solar cell will depend on enhancement of its conversion efficiency. Compared to other inorganic counterparts, it shows low

*Corresponding author.

E-mail address: cheknanali@yahoo.com (A. Cheknane).

efficiency 2.9% or lower. Therefore, more study needs to be done on this cell, while keeping an eye on enhancing its conversion efficiency.

To achieve such goals, a model must be suggested for the MEH-PPV/PCBM organic solar cells. The goal of this work is to find a model that best describes this solar cell. While doing so we revisit a number of earlier models suggested for different types of solar cells. The methodology will be to correlate between earlier experimental photo-current density vs. voltage (J - V) plots, and theoretically constructed (J - V) plots based on different suggested models, under different illumination intensities. Then, a model, that best describes the MEH-PPV/PCBM solar cell, will be suggested based on J - V correlation results.

2. Theory

A major difference between inorganic and organic semiconductors is the exciton binding energy ΔE [24]. It is smaller for Si ($\Delta E \cong 25$ meV, 2.41 kJ/mol) than for organic counterparts ($\Delta E = 300$ meV, 28.95 kJ/mol). Therefore, the exciton is more stable in organics, than in inorganics. Organic solar cell efficiency, η , is typically influenced by the following parameters [25]:

- photon absorption η_A ;
- generation of excitons;
- exciton diffusion η_{diff} ;
- hole–electron separation (exciton dissociation) η_{TC} ;
- carrier transport towards the electrodes (η_{tr});
- charge collection at respective electrodes.

In case of MEH-PPV, it is assumed that the molecules exist in small sized particles. The size and the nature of the particle packing may affect the excitons and their quenching [23].

3. Modeling and simulation

Two equivalent models of the organic solar cell are known.

3.1. The single-diode model

Under illumination, a PV solar cell may be represented by an equivalent circuit, based on a single-diode model, as

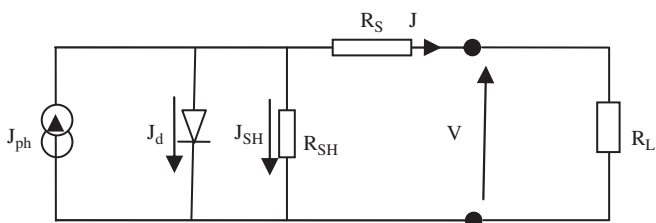


Fig. 1. Equivalent scheme of a real PV cell under illumination, based on a single-diode model [26].

shown in Fig. 1. It is described as a current source in parallel with the junction as follows:

$$J = J_{ph} - \frac{V + JR_s}{R_{sh}} - J_0 \left[\exp \left\{ \frac{q}{nkT} (V + JR_s) \right\} - 1 \right], \quad (1)$$

where J_{ph} is photo-current density; J_0 is the saturation current density under reverse bias, R_s is the series resistance, R_{sh} is the shunt resistance, n is the ideality factor, q is the electronic charge, k is Boltzmann's constant and T is the temperature in Kelvin. The current density (J) is current per unit area.

Series resistance of a given PV solar cell depends on resistivities of the semiconductor bulk, the metal electrodes, and the metal/semiconductor interface. Similarly, in an organic solar cell, the series resistance depends on the resistivities of the organic material(s), the metal electrodes and the metal/organic interface [26]. The series and shunt resistances are linked as follows:

$$J_{sc} = J_{ph} - \frac{J_{sc} R_s}{R_{sh}}. \quad (2)$$

In order to modelize an organic solar cell, Jain and Kapoor [27] presented a new single-diode-based approach using Lambert W -function. The model is shown in Fig. 2.

The processes associated with various blocks in the equivalent circuit diagram of an organic solar cell are: The current source generates current, with a density J_{ph} , upon illumination, which is equal to number of dissociated excitons/s, i.e., number of free electron/hole pairs per second, immediately after generation, before any recombination takes place [27]. The shunt resistor R_{sh} is due to recombination of charge carriers near the dissociation site (e.g. donor/acceptor interface) and it may also include recombination farther away from the dissociation site (e.g. near electrode). The series resistance R_s reflects conductivity, i.e. mobility of specific charge carrier in the respective transport medium, where the mobility is affected by space charges and traps or other barriers (hopping) [27].

3.2. The two-diode model (Mazhari's approach)

Mazhari [28] proposed a two-diode model for organic solar cells, as shown in Fig. 3. R_{sh}^{int} represents loss due to

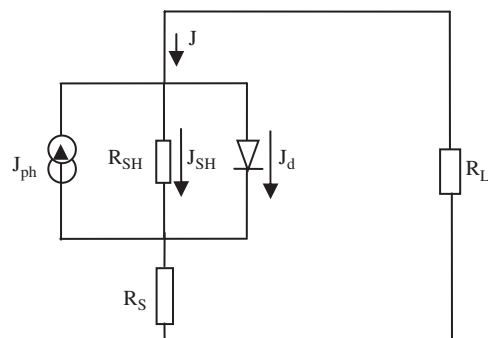


Fig. 2. Equivalent circuit for an organic solar cell (Lambert W -function approach) [27].

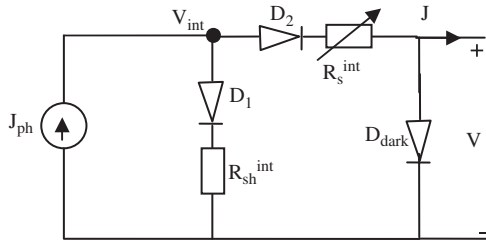


Fig. 3. A simplified equivalent circuit two-diode model for organic solar cells in which losses are modeled in terms of resistances [28].

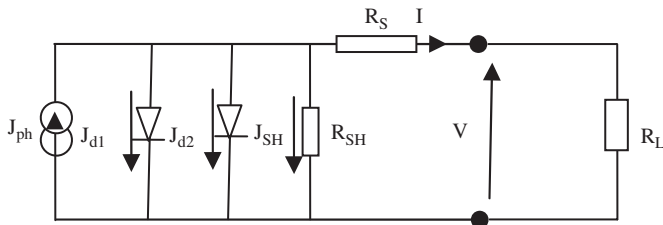


Fig. 4. Equivalent circuit of a two-diode model solar cell [29].

polaron recombination and R_s^{int} models charge extraction to the electrodes. Diodes D_1 and D_2 are ideal diodes that represent short circuit under forward bias and open circuit under reverse bias, respectively.

3.3. An earlier two-diode model

The new simplified equivalent circuit, of a two-diode model solar cell, may be described by the lumped parameter equivalent circuit of Fig. 4, which has been suggested in early 1980s [29,30].

For a given incident light intensity, at a given temperature, the implicit J – V relationship is as follows:

$$J = J_{ph} - \frac{V + JR_s}{R_{sh}} - J_{01}[\exp\{B_1(V + JR_s)\} - 1] - J_{02}[\exp\{B_2(V + JR_s)\} - 1], \quad (4)$$

where $B_1 = q/kT$ and $B_2 = B_1/n$.

J_{01} represents the electronic conduction phenomena in the quasi-neutral region of the junction, such as diffusion, recombination and the drift effect [29], J_{02} corresponds to the carrier recombination via deep levels in the space-charge region of the junction [4]. The reverse saturation current density J_{02} is generally 3–7 orders of magnitude larger than J_{01} [29]; the diode quality factor n equals 2 for the approximation corresponding to the Shockley–Read–Hall recombination current density in the space-charge region [29,31]; n is also a fit parameter that is more than 2.

The experimental study of the temperature dependence of the two terms should help to verify their different origins. Such studies have been published under dark conditions [29,32].

It is of great interest to determine the temperature dependence of parameters J_{01} and J_{02} while the cell is operating as a generator under illumination. It should be noted that illumination does not cause a simple change in current–voltage characteristic along the current axis [29,33]. Moreover, the series resistance effect is non-linear and the injection level goes from a low to a high level.

Differentiation of Eq. (3), while taking into account following equations:

$$R_{sh0} = -\left(\frac{dV}{dJ}\right)_{J=J_{sc}} \quad (4)$$

and

$$R_{s0} = -\left(\frac{dV}{dJ}\right)_{V=V_{oc}} \quad (5)$$

Will yield

$$R_{sh} = \frac{1}{(1/(R_{sh0} - R_s)) - B_1 J_{01} \exp(B_1 J_{sc} R_s) - B_2 J_{02} \exp(B_2 J_{sc} R_s)} \quad (6)$$

and

$$R_s = R_{s0} - \frac{1}{(1/R_{sh}) + B_1 J_{01} \exp(B_1 V_{oc}) + B_2 J_{02} \exp(B_2 V_{oc})}, \quad (7)$$

where R_{s0} and R_{sh0} are the experimental values of the dynamic resistance, which express the behavior of the J – V plot around the open-circuit voltage and around the short-circuit current density points.

For $V = V_{oc}$ and $J = J_{sc}$, we deduce from Eq. (3) that

$$J_{ph} = \frac{V_{oc}}{R_{sh}} + J_{01}[\exp(B_1 V_{oc}) - 1] + J_{02}[\exp(B_2 V_{oc}) - 1] \quad (8)$$

and

$$J_{02} = \frac{(V_{oc}/R_{sh}) - (R_s + R_{sh})J_{sc}/R_{sh} - J_{01}[\exp(B_1 J_{sh} R_s) - \exp(B_1 V_{oc})]}{\exp(B_2 R_s J_{sc}) - \exp(B_2 V_{oc})}. \quad (9)$$

The value of the saturation current density J_{01} is found to be the root of the equation $G(J_{01}) = 0$, where

$$G(J_{01}) = J(MP) - J_{mp}, \quad (10)$$

where J_{mp} is the current density value for experimental maximum power, and $J(MP)$ is the current density value calculated from Eq. (3) for theoretical maximum power.

4. The program

The basic flow of the program needed to resolve the double exponential equation is outlined in Fig. 5. The program was constructed earlier by Charles [29] and is being used her for the MEH-PPV/PCBM organic solar cell system.

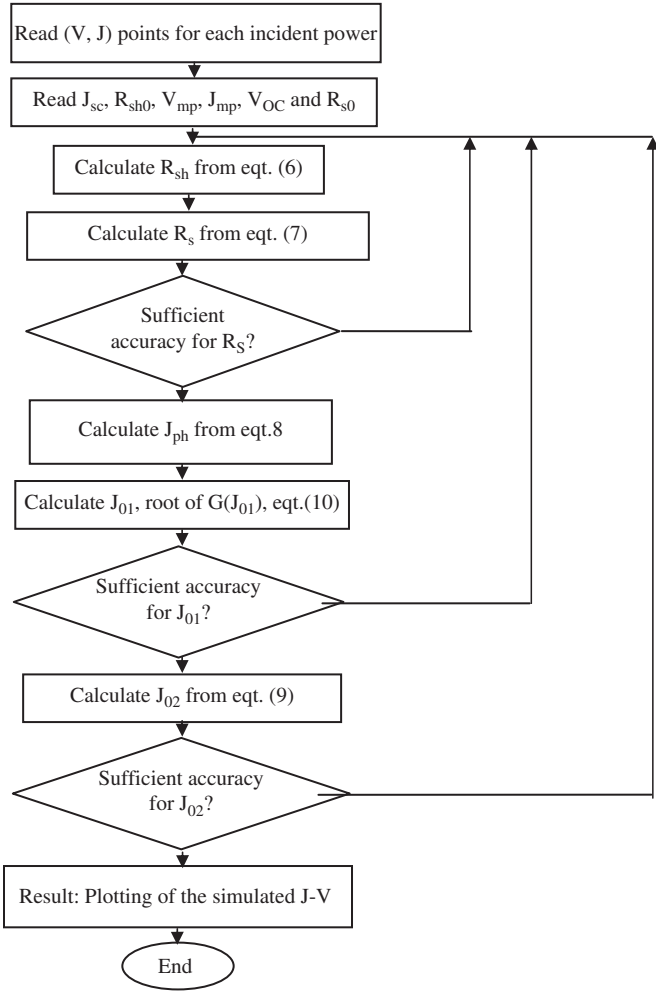


Fig. 5. Flow chart of the program for the resolution of the double exponential equation ($n = 2$).

The program was used as follows:

- 1 The incident power was read.
- 2 From the experimental curve we determined:
 - short-circuit current density;
 - the shunt resistance for $V = 0$, i.e., $1/R_{sh} = -(dJ/dV)_{J=J_{sc}}$; the maximum power from the experimental data allowed to read the corresponding current density and voltage values, J_m and V_m , respectively;
 - from the experimental data we read the open-circuit voltage;
- 3 the series resistance for $J = 0$, i.e., $1/R_{s0} = -(dJ/dV)_{V=V_{co}}$. The series resistance and shunt resistance were calculated as follows:

- (i) for the case where $V = V_{OC}$, $J = 0$
Eq. (3) changes to Eq. (8):
- (ii) for the case where $J = J_{sc}$, $V = 0$, then Eq. (3) becomes

$$J_{sh} = J_{ph} - \frac{J_{sc}R_s}{R_{sh}} - J_{01}[\exp\{B_1(J_{sc}R_s)\} - 1] - J_{02}[\exp\{B_2(J_{sc}R_s)\} - 1]. \quad (11)$$

The differentiation of Eq. (3)/ I , i.e., dJ/dJ

- (i) for the case where $J = 0$, $V = V_{oc}$

$$1 = \left(\frac{dV}{dJ} \Big|_{V=V_{oc}} + R_s \right) \left[-\frac{1}{R_{sh}} - J_{01}B_1[\exp\{B_1(V_{oc})\}] - J_{02}B_2[\exp\{B_2(V_{oc})\}] \right], \quad (12)$$

From Eq. (11), where $R_{s0} = -(dV/dJ)_{V=V_{oc}}$. Thus the R_s is found as shown in Eq. (7).

- (ii) for the case where $V = 0$, $J = J_{sc}$

$$1 = \left(\frac{dV}{dJ} \Big|_{J=J_{sc}} + R_s \right) \left[-\frac{1}{R_{sh}} - J_{01}B_1[\exp\{B_1(J_{sc}R_s)\}] - J_{02}B_2[\exp\{B_2(J_{sc}R_s)\}] \right], \quad (13)$$

where

$$R_{sh0} = - \left(\frac{dV}{dJ} \right)_{J=J_{sc}}.$$

Thus Eq. (6) applies

For $V = V_{OC}$ and $J = J_{sc}$, we deduce Eq. (8) from Eq. (3):

In order to determine R_s , R_{sh} , J_{01} , J_{01} and J_{ph} we may apply two methods:

We put down

1st Method: Eqs. (6)–(8) and (11) form an equation system in with unknowns being R_s , R_{sh} , J_{01} , J_{02} and J_{ph} . To be more general, let

$$\begin{cases} u = R_s, \\ v = R_{sh}, \\ x = J_{ph}, \\ y = J_{01}, \\ z = J_{02}. \end{cases} \quad (14)$$

The system is

$$\begin{cases} f(u, v, x, y, z) = 0, \\ g(u, v, x, y, z) = 0, \\ h(u, v, x, y, z) = 0, \\ \zeta(u, v, x, y, z) = 0, \\ \vartheta(u, v, x, y, z) = 0. \end{cases} \quad (15)$$

To resolve numerically this system we can use the Newton–Raphson algorithm which is shown as

$$\begin{bmatrix} v_k \\ w_k \\ x_k \\ y_k \\ z_k \end{bmatrix} = \begin{bmatrix} v_{k-1} \\ w_{k-1} \\ x_{k-1} \\ y_{k-1} \\ z_{k-1} \end{bmatrix}$$

$$\begin{aligned}
 & - \begin{bmatrix} \frac{\partial f}{\partial u} & \frac{\partial f}{\partial v} & \frac{\partial f}{\partial x} & \frac{\partial f}{\partial y} & \frac{\partial f}{\partial z} \\ \frac{\partial g}{\partial u} & \frac{\partial g}{\partial v} & \frac{\partial g}{\partial x} & \frac{\partial g}{\partial y} & \frac{\partial g}{\partial z} \\ \frac{\partial h}{\partial u} & \frac{\partial h}{\partial v} & \frac{\partial h}{\partial x} & \frac{\partial h}{\partial y} & \frac{\partial h}{\partial z} \\ \frac{\partial \zeta}{\partial u} & \frac{\partial \zeta}{\partial v} & \frac{\partial \zeta}{\partial x} & \frac{\partial \zeta}{\partial y} & \frac{\partial \zeta}{\partial z} \\ \frac{\partial \vartheta}{\partial u} & \frac{\partial \vartheta}{\partial v} & \frac{\partial \vartheta}{\partial x} & \frac{\partial \vartheta}{\partial y} & \frac{\partial \vartheta}{\partial z} \end{bmatrix}^{-1} \\
 & \times \begin{bmatrix} f(u_{k-1}, v_{k-1}, x_{k-1}, y_{k-1}, z_{k-1}) \\ g(u_{k-1}, v_{k-1}, x_{k-1}, y_{k-1}, z_{k-1}) \\ h(u_{k-1}, v_{k-1}, x_{k-1}, y_{k-1}, z_{k-1}) \\ \zeta(u_{k-1}, v_{k-1}, x_{k-1}, y_{k-1}, z_{k-1}) \\ \vartheta(u_{k-1}, v_{k-1}, x_{k-1}, y_{k-1}, z_{k-1}) \end{bmatrix} \quad (16)
 \end{aligned}$$

The initial conditions are chosen as

$$\begin{bmatrix} u(1) \\ v(1) \\ x(1) \\ y(1) \\ z(1) \end{bmatrix} = \begin{bmatrix} 0 \\ 0 \\ 0 \\ 0 \\ 0 \end{bmatrix} \quad (17)$$

2nd Method: The second method, applied in this work, was constructed to determine the maximum power by the derivation of Eq. (3) and equaling it to zero in order to find the $J(\text{MP})$ value corresponding to the maximum power. Therefore, we can calculate J_{01} , which is found to be the root of the equation $G(J_{01}) = 0$, where

$$G(I_{01}) = J(\text{MP}) - J_{\text{mp}},$$

where I_{mp} is the experimental value.

Note that the five different parameters, of the single-diode model, can be determined directly from the latter equations by considering $J_{01} = 0$ and $J_{02} = J_0$, where J_0 is the saturation current density under reversed bias, as defined earlier in Eq. (1) discussions.

- 4 We did testing to have convergence of the solutions.
- 5 We determined the photo-current density.
- 6 We determined J_{01} and J_{02} .
- 7 We used the simulated and the experimental curves to find the best model.

5. Results and discussion

Once the equivalent circuit parameter values were determined, the current density J and the dynamic resistance R for each experimental voltage $V(N)$, were determined. In order to find the model that best describes the organic solar cell, we have constructed simulated $J-V$

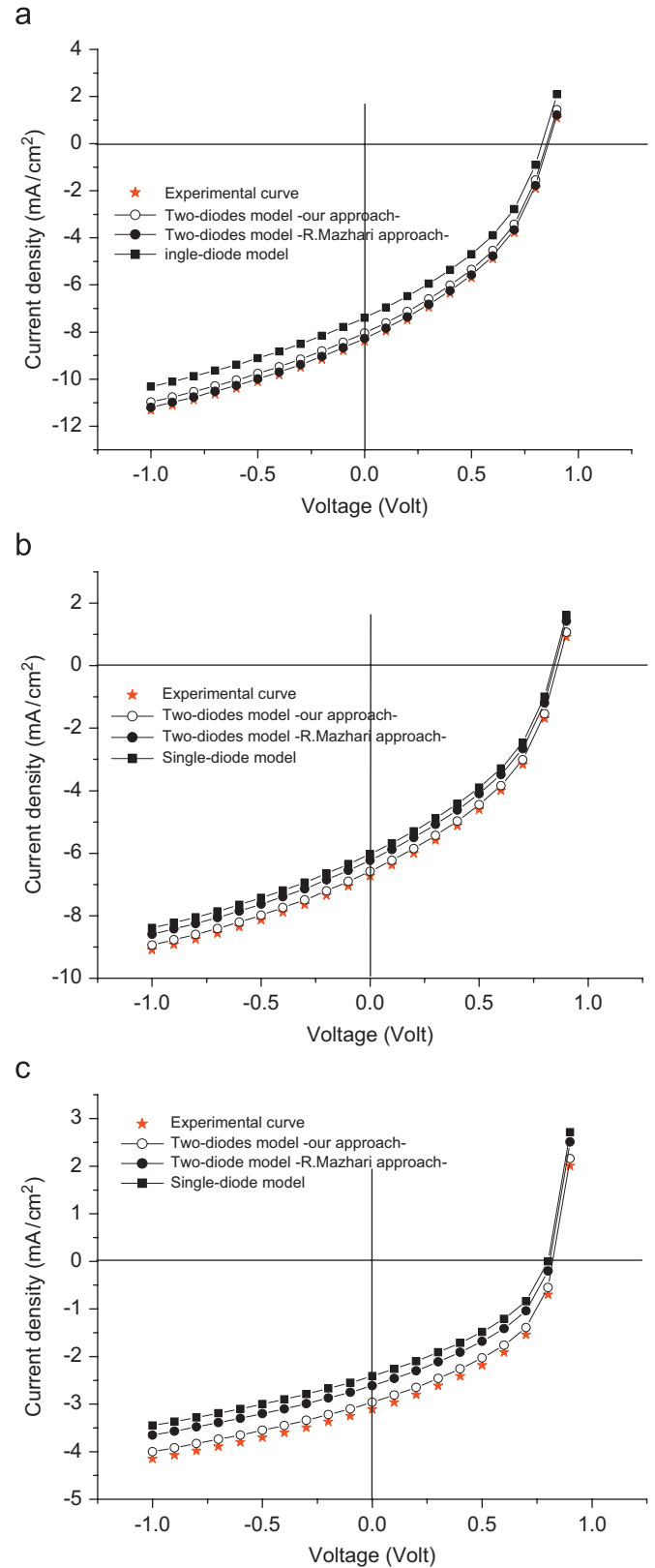


Fig. 6. Simulated curves and experimental measurements of $J-V$ characteristics of the organic solar cell under different illumination intensities: (a) $P_i = 100 \text{ mW/cm}^2$, (b) $P_i = 60 \text{ mW/cm}^2$ and (c) $P_i = 24 \text{ mW/cm}^2$ (where P_i is the incident power density).

Table 1
Calculated parameters based on simulated curves for MEH-PPV/PCBM organic solar cell working under different incident powers: (1) 100 mW/cm², (2) 60 mW/cm² and (3) 24 mW/cm²

Entry no.	Parameter	Incident power	Model			
			Single-diode model	Two-diode model (Mazhari approach)	New two-diode model	Experimental value
(i)	R_s (Ω)	(1)	96.2	93.8	97.7	98 ^a
		(2)	95.2	93.12	97.03	98.65
		(3)	95.002	93.10	96.991	98.85
(ii)	R_{sh} (Ω)	(1)	720	730	734.21	736 ^a
		(2)	718	729.2	734.102	735.25
		(3)	717.12	728.97	733.00	734.12
(iii)	J_{01} (mA/cm ²)	(1)	2.50×10^{-11}	2.4×10^{-11}	2.3×10^{-11}	–
		(2)	2.52×10^{-11}	2.47×10^{-11}	2.32×10^{-11}	–
		(3)	2.55×10^{-11}	2.6×10^{-11}	2.405×10^{-11}	–
(iv)	J_{02} (mA/cm ²)	(1)	6×10^{-7}	78×10^{-6}	5.0×10^{-7}	–
		(2)	6.2×10^{-7}	81×10^{-6}	5.012×10^{-7}	–
		(3)	7.88×10^{-7}	81.2×10^{-6}	5.17×10^{-7}	–
(v)	J_{ph} (mA/cm ²)	(1)	7.2	8.3	8.0	8.3
		(2)	5.9	6.2	6.7	6.8
		(3)	2.3	2.5	3.04	3.2
(vi)	V_{OC} (V)	(1)	0.850	0.8750	0.870	0.875
		(2)	0.790	0.870	0.875	0.875
		(3)	0.81	0.81	0.813	0.813
(vii)	P_m : maximum allowable power output (mW/cm ²)	(1)	2.35	2.86	2.72	2.934
		(2)	1.97	2.094	2.30	2.394
		(3)	0.74	0.846	1.056	1.146
(viii)	FF (%) ($= P_m/V_{OC}, J_{SC}$)	(1)	38.39	39.38	39.08	40.4
		(2)	42.26	38.82	39.23	40.9
		(3)	39.78	41.48	42.73	43.9

FF is the fill factor.

^aCalculated value using the graphical method.

plots based on each model, and compared the simulated plots to the experimental results obtained earlier by Nunzia et al. [12]. Fig. 6(a) shows simulated J – V plots for the organic solar cell based on the single-diode model, the Mazhari's two-diode model and the other earlier two-diode model, as compared to the experimental J – V plot, while working under relatively high illumination intensity (100 mW/cm²). Similarly Fig. 6(a) and (b) show comparative results between simulation and experimental J – V plots under lower illumination intensities, namely 60 and 24 mW/cm², respectively.

The simulated parameters were calculated using the single-diode model, the two-diode model suggested by Mazhari and the earlier two-diode model. Comparison between cell parameters, based on each model with experimental counterparts, was conducted to find the best model. Values of different cell parameters calculated from Fig. 6 are shown in Table 1.

From Table 1, entries (i) and (ii) indicate that the earlier two-diode model, presented here, is the best description for the experimental findings with respect to series resistance

(R_s) and shunt resistance (R_{sh}). The calculated values, based on the earlier two-diode model, resembled the experimental values under all three illumination intensities, more closely than the other models did. Moreover, Mazhari's two-diode approach is better than the single-diode model in calculating the R_s and R_{sh} values.

The photo-current density (J_{ph}) and open-circuit potential (V_{OC}) values calculated from the Mazhari's two-diode approach for 100 mW/cm² illumination intensity resembled the experimental value more closely than the earlier two-diode model. For lower illumination intensities, 60 and 24 mW/cm², the earlier two-diode model showed better fit with experiment, as compared to Mazhari's approach. Under each illumination intensity, the two-diode models gave closer J_{ph} and V_{OC} values to experiment than the single-diode model did. Table 1, entries (v) and (vi), summarizes these trends. Naturally, values of maximum allowed power outputs (P_m) follow same trends, as shown in entry (vii) of Table 1.

Under 100 mW/cm² illumination, the fill factor (FF) simulated values, based on single diode and Mazhari's

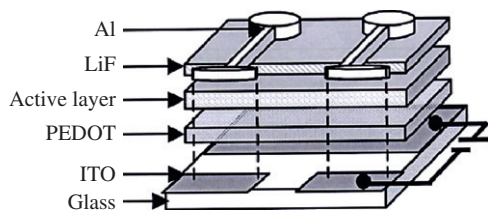


Fig. 7. Device structure of the organic solar cell [12].

two-diode models, showed better resemblance to experiment, than the earlier two-diode approach. At lower illumination intensities, 60 and 24 mW/cm², the earlier two-diode approach showed better fit with experiment than either single-diode or Mazhari's models. These trends are presented in entry (viii) of Table 1.

The results clearly show that the earlier two-diode model, is compatible with the studied organic solar cell for incident powers 24 and 60 mW/cm². On the other hand, the Mazhari's two-diode model seems better for the 100 mW/cm² incident power experiments. In all incident powers used, the single-diode model is less precise in this modelization as compared to either of the two-diode model approaches. The applicability of the earlier two-diode model, is presumably due to the diffusion process of the excitons, which becomes dominating in the conduction mechanisms leading to the generation of carriers in the organics. However, in organic semiconductors and solar cells, the role of excitons is essential, as the primary effect of light absorption is exciton generation, and free electrons and holes are created by exciton dissociation [24].

6. Experimental

We have chosen an organic solar cell, MEH-PPV, with different concentrations of PCBM, as an active layer, which has been described earlier [12]. The preparation of the photovoltaic device, consisting of five layers (Fig. 7) was described earlier [12,34–36]. Using PEDOT between the ITO/glass and the organic active layer enhanced efficiency by increasing open-circuit potential from 0.4 to 0.66 V. Using LiF between the organic active layer and the Al connection increased the short-circuit current, and consequently the current density (Fig. 7). The PEDOT and the LiF increased the cell FF.

7. Conclusions

A earlier two-diode model has been applied here to describe a MEH-PPV/PCBM organic solar cell. The model has been compared to other single-diode and Mazhari's two-diode models, based on resemblance between simulated cell parameters, of each model, and experimental values measured under different illumination intensities. The conventional single-diode model is inadequate to describe the behavior of the organic solar cell. The two-diode models are more appropriate. However, while

Mazhari's approach seems more appropriate for the higher illumination intensity (100 mW/cm²), the earlier two-diode approach is more appropriate for the lower illumination intensities (60 and 24 mW/cm²).

Acknowledgements

We gratefully express our gratitude to Professor Michel Nunzi of "Equipe de Recherche Technologique Cellules Solaires Photovoltaïques Plastiques, Université d'Angers, France", for help.

References

- [1] F.C. Krebs, *Alternative PV: large scale organic photovoltaics*, *Refocus 6* (2005) 38–39.
- [2] K. Kenji, R. Pacios, D. Poplavskyy, Degradation of organic solar cells due to air exposure, *Sol. Energy Mater. Sol. Cells* 90 (2006) 3520–3530.
- [3] R.A.J. Janssen, J.C. Hummelen, N.S. Sariciftci, Theme article-polymer–fullerene bulk heterojunction solar cells, *MRS Bull.* 30 (2005) 33.
- [4] C.J. Brabec, J.A. Hauch, P. Schilinsky, C. Waldauf, Theme article-production aspects of organic photovoltaics and their impact on the commercialization of devices, *MRS Bull.* 30 (2005) 50.
- [5] K.M. Coakley, M.D. McGehee, Conjugated polymer photovoltaic cells, *Chem. Mater.* 16 (2004) 4533–4542.
- [6] H. Spanggaard, F.C. Krebs, A brief history of the development of organic and polymeric photovoltaics, *Sol. Energy Mater. Sol. Cells* 83 (2004) 125–146.
- [7] S.E. Shaheen, C.J. Brabec, N.S. Sariciftci, F. Padinger, T. Fromherz, J.C. Hummelen, 2.5% efficient organic plastic solar cells, *Appl. Phys. Lett.* 78 (2001) 841.
- [8] N.S. Sariciftci, D. Braun, C. Zhang, V.I. Srdanov, A.J. Heeger, G. Stucky, F. Wudl, Semiconducting polymer–buckminsterfullerene heterojunctions: diodes photodiodes, and photovoltaic cells, *Appl. Phys. Lett.* 62 (1993) 585.
- [9] G. Yu, J. Gao, J.C. Hummelen, F. Wudl, A.J. Heeger, Polymer photovoltaic cells: enhanced efficiencies via a network of internal donor–acceptor heterojunctions, *Science* 270 (1995) 1789.
- [10] C.J. Brabec, F. Padinger, N.S. Sariciftci, J.C. Hummelen, Photovoltaic properties of conjugated polymer/methanofullerene composites embedded in a polystyrene matrix, *J. Appl. Phys.* 85 (1999) 6866–6872.
- [11] D. Gebeyehu, C.J. Brabec, F. Padinger, T. Fromherz, J.C. Hummelen, D. Badt, H. Schindler, N.S. Sariciftci, The interplay of efficiency and morphology in photovoltaic devices based on interpenetrating networks of conjugated polymers with fullerenes, *Synth. Met.* 118 (2001) 1.
- [12] S. Alem, R. de Bettignies, J.-M. Nunzi, Efficient polymer-based interpenetrated network photovoltaic cells, *Appl. Phys. Lett.* 84 (2004) 2178–2180.
- [13] G. Yu, J. Gao, J.C. Hummelen, F. Wudl, A.J. Heeger, Polymer photovoltaic cells: enhanced efficiencies via a network of internal donor–acceptor heterojunctions V, *Science* 270 (1995) 1789–1791.
- [14] C. Yang, H. Li, Q. Sun, J. Qiao, Y. Li, Y. Li, D. Zhu, Photovoltaic cells based on the blend of MEH-PPV and polymers with substituents containing C₆₀ moieties, *Sol. Energy Mater. Sol. Cells* 85 (2005) 241–249.
- [15] Q. Shi, Y. Hou, Jing Lu, H. Jin, Y. Li, Y. Li, X. Sun, J. Liu, Enhancement of carrier mobility in MEH-PPV film prepared under presence of electric field, *Chem. Phys. Lett.* 425 (2006) 353–355.

- [16] P.M. Sirimanne, E.V.A. Premalal, P.K.D.D.P. Pitigala, K. Tennakone, Utilization of MEH-PPV as a sensitizer in titania-based photovoltaic cells, *Sol. Energy Mater. Sol. Cells* 90 (2006) 1673–1679.
- [17] A. Kumar, P.K. Bhatnagar, P.C. Mathur, K. Tada, M. Onoda, Improved electrical and optical properties of MEH-PPV light emitting diodes using Ba buffer layer and porphyrin, *Appl. Surf. Sci.* 252 (2006) 3953–3955.
- [18] D.H. Choi, M.J. Cho, K.I. Han, I.-H. Chang, J.S. Song, J.H. Kim, S.-H. Paek, S.-H. Choi, Luminescence properties of MEH-PPV and its crosslinked polymer: effect of crosslink on photoluminescence and electroluminescence, *Synth. Met.* 156 (2006) 685–689.
- [19] Sh. Quan, F. Teng, Z. Xu, L. Qian, Y. Hou, Y. Wang, X. Xu, *Eur. Polym. J.* 42 (2006) 228–233.
- [20] A.K. Biswas, A. Tripathi, S. Singh, Y.N. Mohapatra, Effect of condensed phase environment on luminescent properties of MEH-PPV thin films, *Synth. Met.* 155 (2005) 340–343.
- [21] O. Mirzov, T. Pullerits, F. Cichos, C. von Borczyskowski, I.G. Scheblykin, Large spectral diffusion of conjugated polymer single molecule fluorescence at low temperature, *Chem. Phys. Lett.* 408 (2005) 317–321.
- [22] O. Mirzov, F. Cichos, C. von Borczyskowski, I. Scheblykin, Fluorescence blinking in MEH-PPV single molecules at low temperature, *J. Lumin.* 112 (2005) 353–356.
- [23] O. Mirzov, F. Cichos, C. von Borczyskowski, I.G. Scheblykin, Direct exciton quenching in single molecules of MEH-PPV at 77 K, *Chem. Phys. Lett.* 386 (2004) 286–290.
- [24] M. Burgelman, B. Minnaert, Including excitons in semiconductor solar cell modelling, *Thin Solid Films* 511–512 (2006) 214–218.
- [25] A. Moliton, J.-M. Nunzi, How to model the behaviour of organic photovoltaic cells, *Polym. Int.* 55 (2006) 583–600.
- [26] J.M. Nunzi, *Organic Materials and Devices For Photovoltaic applications*, ERT Cellules Solaires Photovoltaïques Plastiques, Labo POMA, Angers, France, 2002, pp. 197–224.
- [27] A. Jain, A. Kapoor, A new approach to study organic solar cell using Lambert W -function, *Sol. Energy Mater. Sol. Cells* 86 (2005) 197–205.
- [28] B. Mazhari, An improved solar cell circuit model for organic solar cells, *Sol. Energy Mater. Sol. Cells* 90 (2006) 1021–1033.
- [29] J.-P. Charles, *Caractérisation $i(v)$ et fonctionnement des photopiles solaires*, Thèse de Doctorat ès Sciences, Université des Sciences et Techniques du Languedoc, Juillet 1984.
- [30] G.L. Araujo, E. Sanchez, M. Marti, Determination of the two-exponential solar cell equation parameters from empirical data, *Sol. Cells* 5 (1982) 199–204.
- [31] J.-P. Charles, A. Haddi, A. Maouad, H. Bakhtiar, A. Zerga, A. Hoffmann, P. Mialhe, La jonction du solaire à la Microélectronique, *Rev. Energy Ren.* 3 (2000) 1–16.
- [32] M. Wolf, G.T. Noel, R.J. Stirn, *IEEE Trans. Electron. Dev.* ED-24 (4) (1977) 419–428.
- [33] R.N. Hall, Silicon photovoltaic cells, *Solid-State Electron.* 24 (1981) 595–616.
- [34] J.C. Hummelen, B.W. Knight, F. LePeq, F. Wudl, J. Yao, C.L. Wilkins, Preparation and characterization of fulleroid and methanofullerene derivatives, *J. Org. Chem.* 60 (1995) 532–538.
- [35] C.J. Brabec, S.E. Shaheen, C. Winder, N.S. Sariciftci, P. Denk, Effect of LiF/metal electrodes on the performance of plastic solar cells, *Appl. Phys. Lett.* 80 (2002) 1288–1290.
- [36] G.E. Jabbour, B. Kippelen, N.R. Amsrtong, N. Peyghambarian, Aluminum based cathode structure for enhanced electron injection in electroluminescent organic devices, *Appl. Phys. Lett.* 73 (2002) 1185–1187.